Sensors & Actuators: A. Physical 393 (2025) 116780

Contents lists available at ScienceDirect

Sensors and Actuators: A. Physical

journal homepage: www.journals.elsevier.com/sensors-and-actuators-a-physical

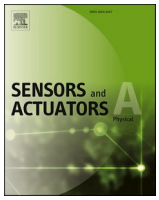

Detecting, quantifying and distinguishing malarial species with surface plasmon microscope

Ipsita Chakraborty [*,1], Justus Bednar, Andreas Offenhäusser [2]

Institute of Biological Information Processing, Juelich Research Center, Wilhelm-Johnen-Strasse, Juelich 52428, Germany

ARTICLE INFO

Keywords:
Plasmodium falciparum
Plasmodium vivax
Malaria
Refractive index
Surface plasmon
Microscope
Label-free

ABSTRACT

In this work we develop a refractive index-based methodology with a surface plasmon microscope to detect, then quantize and eventually differentiate various malarial species in human whole blood. A nanometric flat metal surface can support surface plasmons. The plasmon propagates along the metal surface with a propagation constant that reveals a direct dependency on a refractive index in the optical near field of the surface. This surface plasmon microscope is a sensitive measurement probe for the refractive index with standard deviation $\sim 10^{-4}$ on the metal surface. Whole blood samples from patients infected with malaria were evaluated. The quantification of unprocessed whole blood infected with 2000 parasites/μl of *Plasmodium falciparum* and *Plasmodium vivax* species revealed significant differences in refractive index $\sim 10^{-1}$ AU. While that with 200 parasites/μl of *Plasmodium falciparum* and *Plasmodium vivax* species revealed differences in refractive index $\sim 10^{-2}$ AU.

1. Introduction

249 million cases of malarial incidences were reported from 85 countries in 2022. While 29 countries accounted for 95 % of malaria cases. Four countries – Nigeria (27 %), the Democratic Republic of the Congo (12 %), Uganda (5 %) and Mozambique (4 %) accounted for almost half of all cases globally. Estimated 608,000 deaths (79 % reported in Africa) were related to malaria in 2022, of which 76 % were children under the age of five [1].

Malaria starts with the injection of plasmodium sporozoites into the dermis of an individual by female Anopheles mosquito [2]. After the parasite enters the human body, it infects liver cells [3], reproduces, multiplies and subsequently infects blood vessels. Eventually infected red blood cells rupture after undergoing four distinct stages of development and release new parasites [4]. This repeated cycle leads to high fever and chills in the affected individual [5]. Four species namely *Plasmodium falciparum*, *Plasmodium vivax*, *Plasmodium malaria,* and *Plasmodium ovale* are considered true parasites to humans while others (*Plasmodium knowlesi*) are mostly zoonotic. In Africa, *Plasmodium falciparum* is the most prevalent malarial parasite, accounting for 99.5 % of cases versus the 0.5 % of cases caused by *Plasmodium vivax*, while in Asia, 50.9 % of cases are caused by *Plasmodium vivax* and 49.1 % of cases are caused by *Plasmodium falciparum* [6,7].

Early diagnosis is the key factor to reduce mortality in malaria infected patients. Malaria is often diagnosed by microscopic examination of stained blood films using Field's stains. However, low parasitemia often leads to misdiagnosis, hence in some instances artificial assisted technologies are gaining importance [8]. The quantitative buffy coat (QBC) approach, which uses blood staining and an epifluorescence microscope to identify malaria, is intended to enhance microscopic malaria diagnosis [9]. However, the QBC method cannot be used for quantifying malarial parasites. Hence, rapid diagnostic tests (RDTs) based on parasite antigens have been proposed [10,11]. Polymerase chain reaction (PCR)-based technique is a highly sensitive method of diagnosis relying on the amplification of specific sequences of DNA of the malarial parasite [12]. PCR technology is restricted due to high costs, the requirement of trained professionals and specific instruments. While loop-mediated isothermal amplification (LAMP) based on the turbidity detection of the DNA sequences can be an affordable alternative to PCR [13]. Microarrays also play an important role in the diagnosis of infectious diseases that are based on fluorescence measurement during DNA hybridization [14]. Even, flow cytometry (FCM) based on

* Corresponding author.
E-mail address: i.chakraborty@fz-juelich.de (I. Chakraborty).
[1] 0009–0003–5521–1008
[2] 0000–0001-6143–2702

https://doi.org/10.1016/j.sna.2025.116780
Received 15 November 2024; Received in revised form 14 May 2025; Accepted 5 June 2025
Available online 7 June 2025

hemozoin detection has been reported for malaria diagnosis. [15]. Also, mass spectrometry (MS) based on identification of hemozoin by laser desorption mass spectrometry (LDMS) has been used [16]. Further various aptamer-based sensors have also been developed for detecting malaria [17].

Nonetheless, the quest for label-free techniques for quantitative malarial species detection particularly for low parasitemia continues. In this regard surface plasmon sensors exquisite capabilities have been sought for decades. Notable advances in PCR fiber sensors for malaria detection have been reported [18]. However, PCR fiber sensors require rigorous design for optimization based on specific applications. In this regard advancements have been made in wave-flex biosensors as well [19–22].

Surface plasmon, or collective electron oscillations, can be supported by a flat metal surface. In the optical near field, the surface plasmon propagates along the metal surface with a propagation constant that indicates a substantial dependence on the refractive index. Surface plasmons have been considered as one of the most sensitive tools for label-free detection [23]. When p-polarized light is incident at a particular angle on a nanometric metal coated glass substrate, surface plasmons are excited. As surface plasmons absorb energy, confirmed by the sharp fall in the reflected intensity with the spatial frequency of incident illumination. The spatial frequency corresponding to the reflectance minima is termed as the propagation constant. The measurement sensitivity is a function of the full width at half maxima (FWHM) of the reflectance spectra. In the visible wavelength range, the sharpest dip can be observed with nanometric silver coated glass substrates followed by nanometric gold coated glass substrates [24]. However, silver is easily prone to environmental and chemical changes (oxidation) leading to sensitivity degradation. There are two ways to mitigate the shortcomings, one by coating a protective silica layer on top of nanometric silver [25], or by coating a polymer film [26] such as PMMA (poly-methyl methacrylate) to endure the environmental changes specifically suitable for long term biological experiments.

Surface plasmon microscopy has also been demonstrated for characterizing the isotropic properties such as refractive index as well as anisotropic properties like linear birefringence. For isotropic samples the reflected spatial frequency distribution is circular in nature. The magnitude of the circular pattern can be correlated with the refractive index of the sample [27]. For uniaxial samples, the magnitude of birefringence can be obtained from the distortion in the shape of the reflected spatial frequency distribution (eccentricity) while the rotation of the absorption pattern is a measure of the orientation of its fast axis [28–31]. The potential of this surface plasmon microscope can also be used towards the pre-clinical diagnosis of different types of diseases [32]. Hence, this microscope can be used to not only detect [33] malarial species but also to quantify and differentiate between them. Moreover, the minimum sample requirement is in atto-liter [34] and can even be used when studying the evaporating dynamics of biofluid which is not feasible with conventional Abbe refractometers [35]. For extremely costly biological samples such as samples collected from Alzheimer's patients this minimum volume requirement can be extremely beneficial.

In this paper we utilize the surface plasmon microscope to detect, quantify and differentiate two malarial species namely *Plasmodium falciparum* and *Plasmodium vivax* in whole human blood. This is conducted in a label free manner by extracting the refractive indices of whole blood as well as that of various malarial species infected whole blood. We evaluate the refractive index by correlating the radius of the absorption pattern from the spatial frequency distribution of the high numerical aperture objective lens. This provides a quantitative method to determine parasitemia as well as give an estimate of the malarial species. This label-free approach might serve as a useful method for the simultaneous quantization of parasitemia as well as differentiating malarial species.

2. Methods and experimental analysis

2.1. Substrate preparation and characterization

N-LAF21 (r.i.: 1.7845, Olympus) coverslips were cleaned with ethanol, acetone, and isopropanol for 5 mins each. Then the coverslips were subjected to oxygen plasma for 5 mins. Later, chromium layer (~3 nm, r.i.: 3.1361 + i3.312) followed by gold layer (~ 40 nm, r.i.: 0.2038 + i3.318) were deposited by E-beam vapor deposition as shown in Fig. 1(a). The chromium nanometric layer was added for a better adhesion of the gold nanometric layer. The thickness of the subsequent layers was analyzed with X-ray reflectometry (XRR). Kiessig fringes are an interference pattern that arises from the reflections of subsequent layers of the sample under test. The period of these fringes and the fall in intensity are related to the thickness and roughness of the subsequent layers. The thickness of the nanometric gold layer as embedded in the Kiessig fringes was observed as shown in Fig. 1(b). The thickness was evaluated with GenX3 [36]. The analysis revealed the atomic densities for the chromium and gold layers were 0.0833 gcm^{-3} and 0.0590 gcm^{-3} respectively, while the average roughness of the chromium and gold nanometric layers were 8.48 Å and 11.20 Å respectively, the thickness obtained for the chromium and the gold nanometric layers were 3.04 nm and 40.04 nm respectively.

2.2. Working of the surface plasmon microscope

A He-Ne laser ($\lambda = 632.8$ nm, 5 mW) was used as a light source. The linearly polarized laser beam was collimated by a beam expander and subsequently converted to radially polarized beam with z-pol (Nanophoton). The collimated beam was introduced to a microscope objective (special oil-immersion, 100 × magnification, NA 1.70, Olympus, APON100XHOTIRF), and was tightly focused on the gold thin film through the cover slip. The focused laser beams excited surface plasmons on the metal surface facing the sample. The laser beam reflected from the gold film was collected by the same objective lens. The Fourier spectrum of the reflected light, which was created at the objective's exit pupil, was observed by CCD1 after reflection from a cube beamsplitter. We observed the PSF of the incident laser beam with CCD2 after reflection from the cube beam splitter. Also, the system was integrated with vertical microscope objective (20 × magnification, NA 0.8, Olympus, UPLXAPO20X). The sample was imaged with CCD3.

When the resonant angle of the surface plasmon was within the angular semi-aperture of the objective lens, a certain component of the reflected light was absorbed by the surface plasmon, and as a result, a

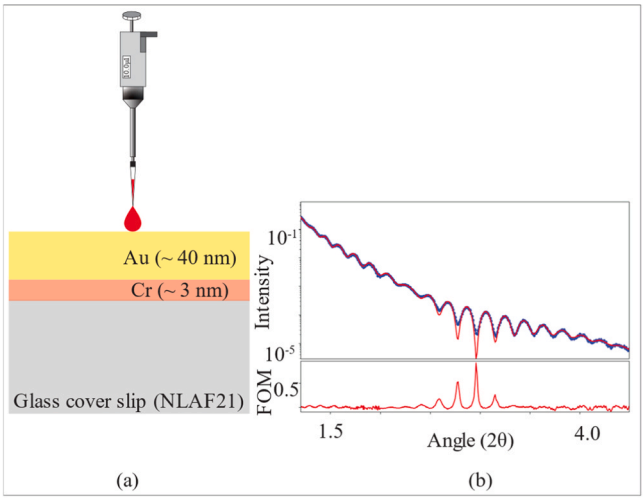

Fig. 1. (a) Substrate configuration, (b) Determination of the thickness of nanometric gold layer from Kiessig fringes with XRR.

dark ring (hence referred to as circular absorption pattern) was created in the Fourier image. When the sample attached to the gold film was isotropic, the shape of the absorption pattern was completely circular because of the rotational symmetry of the system. Since the radius of the ring corresponded to the resonant angle of the surface plasmon and the resonant angle was directly associated with the refractive index of the sample, the system could measure the absolute value of the sample's refractive index from the reflected spatial frequency distribution or the Fourier image. Using this setup, we measured the reflected spatial frequency distributions from the blood samples on the substrate.

2.3. Refractive index analysis and sensitivity measurement with the surface plasmon microscope

We assume a substrate in Kretschmann configuration consisting of a coverslip with multi-layered coating. The surface plasmons are excited on the Au-blood interface by radially polarized incident beam. We analyze the reflected spatial frequency distribution of the recorded exit pupil of the high numerical aperture objective lens.

In this regard we position and scale a polar coordinate system onto exit pupil plane images (CCD1 in Fig. 2), while the corresponding angles of light reflection in the sample plane are calculated pixel-by-pixel. The median light intensity of each reflection angle is calculated, resulting in an intensity-angle spectrum. A stratified layer model is employed to fit a transfer-matrix-method [37] prediction of the reflectance-angle spectrum, comparing the intensity-angle spectrum with a previously characterized illumination-angle spectrum. This approach allows for the retrieval of the blood refractive index parameter through a single-parameter least-square optimization. The software for data analysis, developed in-house, is publicly available for download from [38].

In this regard we analyzed the sensitivity of the surface plasmon microscope with artificial blood (BZ410 from Biochemazone) at various temperatures as shown in Fig. 3, to show the variation of the measurement. The measurement was performed on a weekly basis to demonstrate the sensitivity of the surface plasmon microscope.

The standard deviation in R.I. measurement as recorded with this microscope was $\sim 10^{-4}$ A.U. It should be noted that all refractive index analysis was performed on the same day when the substrates were prepared to negate any environmental degradation of the substrates on sample measurements. Also, the surface plasmon probe was calibrated on the day of measurement with artificial blood (BZ410 from Biochemazone) as shown in Fig. 4. to accurately determine the refractive index of the sample under test. Moreover, the experiment was conducted in maintained room temperature of 21°C to negate any refractive index changes arising from the environmental conditions.

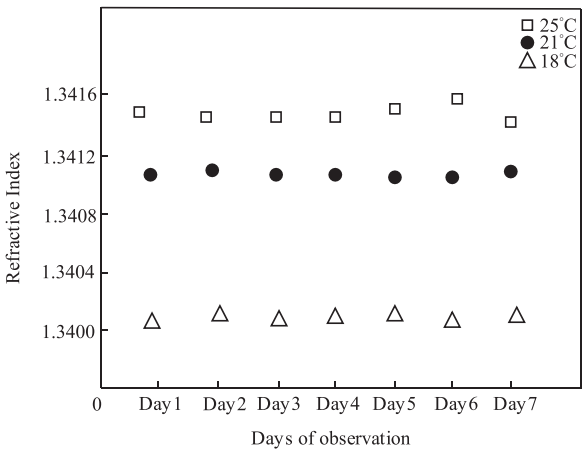

Fig. 3. Weekly refractive index analysis of artificial blood at three different temperatures.

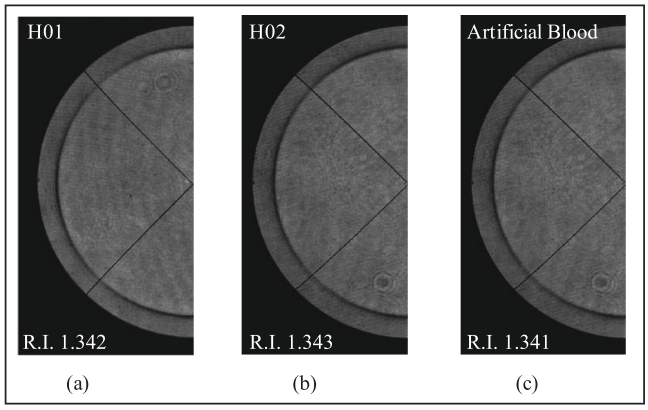

Fig. 4. (a) Exit pupil image of whole blood H01 (Individual not infected with malaria), (b) Exit pupil image of whole blood H02 (Individual not infected with malaria), (c) Exit pupil image of artificial blood.

2.4. Analyzing whole blood samples from healthy individuals

10 µl of whole blood was pipetted on top of the substrate as illustrated in Fig. 1(a). Later, the exit pupil plane images of the high numerical aperture objective lens were recorded. The data was processed with in-house software written in Python as discussed in Section 2.3. Table 1 below shows the extracted values of the refractive indices as

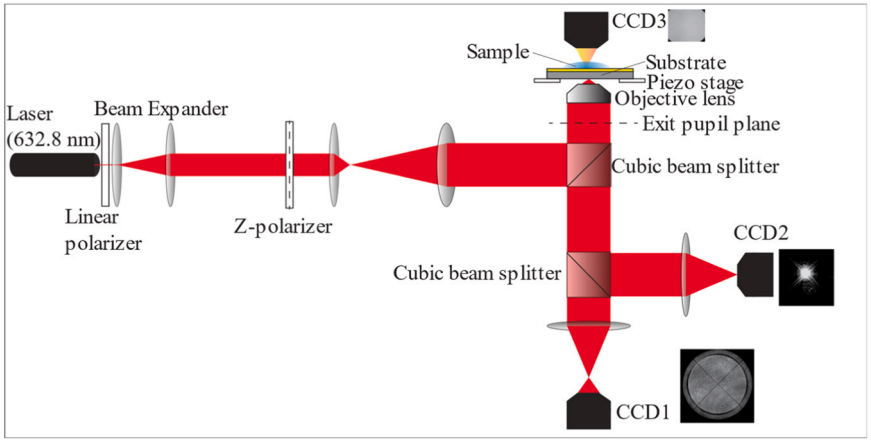

Fig. 2. Experimental setup for the development of the surface plasmon microscope.

Table 1
Refractive index of whole blood of individuals not affected with malaria.

Sample code	Age of individual	Refractive index
H01	21 yrs old female	1.342
H02	20 yrs old female	1.343
Artificial blood (AB)	——	1.341

obtained by analyzing the exit pupil. We also evaluated the refractive index of artificial blood at 632.8 nm for calibration purposes, and the result is shown in the last column of Table 1. All data were recorded at 21°C (maintained room temperature throughout the experiment).

Fig. 4 shows a portion of the exit pupil images as obtained with whole blood from individuals not affected with malaria and with artificial blood. As analyzed, the R.I. of whole blood of two female volunteers' whole blood were 1.342 and 1.343 respectively.

From the two healthy whole blood samples the variability of refractive index ~ 10^{-3} was recorded. Further the experiment was repeated to analyze the reproducibility of the results. We found that the standard deviation of the variability of the same measurement in the refractive index ~10^{-4}.

2.5. Calibration curve for whole blood samples infected with malaria

We used whole blood samples F01 and V01 containing 2000 parasites/μl of *Plasmodium vivax* and *Plasmodium falciparum* species respectively and added artificial blood to obtain ordered parasitemia. We analyzed those blood samples after pipetting the same on the substrate as shown in Fig. 1(a). Table 2 shows the preparation methodology of blood samples. For each case two samples were prepared to analyze the degree of variability in the measurements. Also, one must be careful regarding the ambient room temperature while preparing and measuring the samples. In our case an ambient temperature of 21°C was maintained throughout. Further to explain the suitability of this measurement method, samples with low parasitemia (up to ~ 16 parasites/μl) were prepared.

Fig. 5 shows the calibration curve for the whole blood samples as prepared for various levels of parasitemia with *Plasmodium falciparum* and *Plasmodium vivax*.

As shown in Fig. 5, using this measurement approach we were able to distinguish between Plasmodium species with low parasitemia (~16 parasites/μl). Even though we could detect refractive index changes in Plasmodium species for ~16 parasites/μl, we feel the variability of refractive index in healthy blood samples from different individuals may interfere with this margin (even though variability of refractive index was much lower as recorded by us as shown in Fig. 4). Further we would like to emphasis on the fact that refractive index changes in healthy individuals are extremely low as (shown in Fig. 4) ~10^{-3}, while that obtained with Plasmodium species are in ~ 10^{-2}. In this case we conclude that Plasmodium species with 60 parasites/μl or above can be reliably distinguished based on refractive index changes if the system standard deviation is < 10^{-4}.

Table 2
Preparation of blood samples with different parasitemia for Plasmodium falciparum and plasmodium vivax species.

Sample code	Addition of artificial blood	Plasmodium parasites/μl
F01–1,2	0	2000
F02–1,2	0.75 μl added /μl of F01	1500
F03–1,2	1 μl added /μl F01	1000
F04–1,2	1 μl added /μl F03	500
F05–1,2	1 μl added /μl F04	250
F06–1,2	9 μl added /μl F01	200
F07–1,2	1 μl added /μl F05	125
F08–1,2	1 μl added /μl F07	63
F09–1,2	1 μl added /μl F08	32
F10–1,2	1 μl added /μl F09	16
V01–1,2	0	2000
V02–1,2	0.75 μl added /1 μl V01	1500
V03–1,2	1 μl added to /μl V01	1000
V04–1,2	1 μl added to /μl V03	500
V05–1,2	1 μl added to /μl V04	250
V06,1–2	9 μl added /μl V01	200
V07,1–2	1 μl added /1 μl V05	125
V08,1–2	1 μl added /1 μl V07	63
V09,1–2	1 μl added /1 μl V08	32
V10,1–2	1 μl added /1 μl V09	16

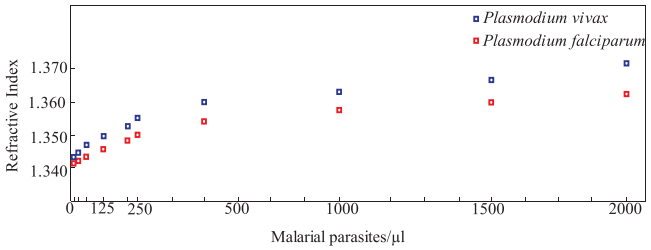

Fig. 5. Calibration curve for samples as shown in Table 2 for various concentrations of malarial parasites *Plasmodium vivax* and *Plasmodium falciparum* shown in blue and red respectively.

Plasmodium falciparum/ Plasmodium vivax refractive indices and the relevant parasitemia can be fitted with suitable statistics such as logarithmic or power series. We obtained R_1=1.3207$P_1^{0.004}$ with index of correlation as 0.97 (for null hypothesis) or $R_1 = 0.065 \ln(P_1) + 1.3202$ with index of correlation index 0.97 (Spearman's correlation coefficient) where R_1 represents the refractive index and P_1 the parasitemia value (parasites/μl) for *Plasmodium vivax*. Further, we obtained R_2=1.3211$P_2^{0.004}$ with index of correlation as 0.99 or $R_2 = 0.0054 \ln(P_2) + 1.3207$ with correlation index as 0.99 (Spearman's correlation coefficient), where R_2 represents the refractive index and P_2 the parasites/μl) for *Plasmodium falciparum*. These statistics may later serve as a guide for very quick analysis of presence or absence and quantification of the malarial species from the refractive index of whole blood. After obtaining the calibration curve we analyzed whole blood samples with individuals infected with malaria.

2.6. Analyzing whole blood samples from individuals infected with malaria

We further analyzed the whole blood of individuals infected with *Plasmodium falciparum* species. Again, 10 μl of whole blood was pipetted on top of the substrate as illustrated in Fig. 1(a). Table 3 shows the refractive index values as obtained by analyzing the exit pupil.

Fig. 6 shows a portion of the exit pupil images obtained with whole blood from individuals affected with *Plasmodium falciparum*. As analyzed, the R.I. of whole blood infected with 2000 *Plasmodium falciparum* parasites/μl and 200 *Plasmodium falciparum* parasites/μl were 1.362 and 1.349 respectively. As evidenced in Table 2, whole blood samples from four individuals affected with *Plasmodium falciparum* were analyzed and even then, the refractive index variability was found ~10^{-3} for a particular level of parasitemia. Once again, indicating that the refractive index changes are extremely low for different individuals.

We further analyzed the whole blood of individuals infected with *Plasmodium vivax* species. Again, 10 μl of whole blood was pipetted on

Table 3
Refractive index of whole blood of individuals affected with *Plasmodium falciparum*.

Sample code	Age of individual	Refractive index
F01–3	22 yrs old female	1.362
F01–4	21 yrs old female	1.365
F06–3	21 yrs old female	1.349
F06–4	20 yrs old female	1.346

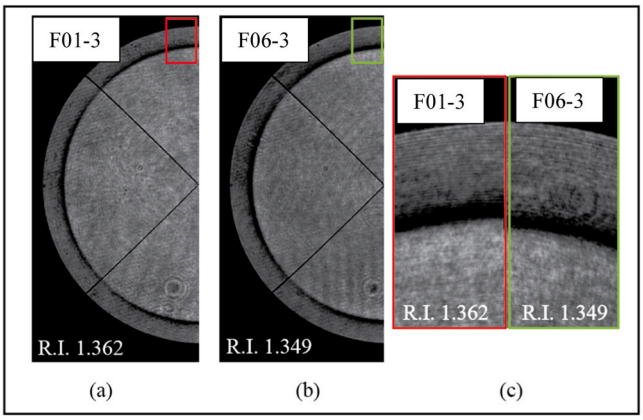

Fig. 6. (a) Exit pupil image of whole blood F01–3 (with 2000 *Plasmodium Falciparum* parasites/μl), (b) Exit pupil image of whole blood F06–3 (with 200 *Plasmodium falciparum* parasites/μl), (c) Comparison of selected portions in red and green squares of (a) and (b) reveal absorption pattern differences.

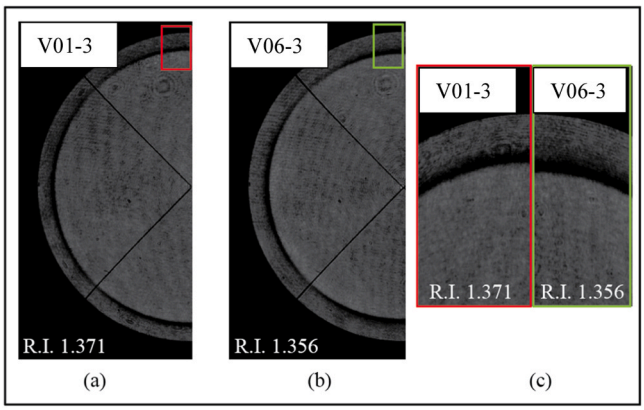

Fig. 7. (a) Exit pupil image of whole blood V01 (with 2000 *Plasmodium vivax* parasites/μl), (b) Exit pupil image of whole blood V06 (with 200 *Plasmodium vivax* parasites/μl), (c) Comparison of selected portions in red and green squares of (a) and (b) reveal absorption pattern differences.

top of the substrate as illustrated in Fig. 1(a). Table 4 shows the refractive index values as obtained by analyzing the exit pupil.

Fig. 7 shows a portion of the exit pupil images as obtained with whole blood from individuals affected with *Plasmodium vivax*. As analyzed, the R.I. of whole blood infected with 2000 *Plasmodium vivax* parasites/μl and 200 *Plasmodium vivax* parasites/μl were 1.371 and 1.356 respectively. As evidenced in Table 2, whole blood samples from four individuals affected with *Plasmodium vivax* were analyzed and even then, the refractive index variability was found $\sim 10^{-3}$ for a particular level of parasitemia. Moreover, all the samples were analyzed at least twice to showcase the reproducibility of the results with this measurement approach. Standard deviations in results obtained with same samples $\sim 10^{-4}$.

Apparently, as shown in Figs. 6 and 7, there exists a remarkable refractive index variability in blood infected with *Plasmodium vivax* and *Plasmodium falciparum* (even with same parasitemia). Further the changes in the refractive index are quantifiable for various plasmodium species.

Fig. 8 shows the variation of the refractive index as mapped with samples F01–3, F01–4 and F06–3, F06–4 containing *Plasmodium falciparum* species in the range of 2000 parasites/μl and 200 parasites/μl respectively marked in red, while V01–3, V01–4 and V06–3, V06–4 containing *Plasmodium vivax* species in the range of 2000 parasites/ μl and 200 parasites/μl marked in blue. Further in the background of Fig. 8, plotted with dashed lines in red and blue are the calibration curves for *Plasmodium falciparum* and *Plasmodium vivax* respectively.

Fig. 8 also reveals another important part of the study regarding the variation of the refractive index arising from different patients infected with malaria. As evidenced before, the change in refractive index for the various patients was extremely low. Even considering the variability of the patients, the calibration curves can be used to predict the parasitemia levels as well as the malarial species of origin. Given the samples evaluated for this study were low, further investigations with large cohort size are required to establish this fact in general. Also, we were concerned with the two predominant malarial species, i.e. *Plasmodium falciparum* and *Plasmodium vivax* (given 90 % of infections occurs from single species incidence [6,7]) and have not considered mixed species

Table 4
Refractive index of whole blood of individuals affected with *Plasmodium vivax*.

Sample code	Age of individual	Refractive index
V01–3	21 yrs old female	1.371
V01–4	21 yrs old female	1.373
V06–3	20 yrs old female	1.356
V06–4	21 yrs old female	1.354

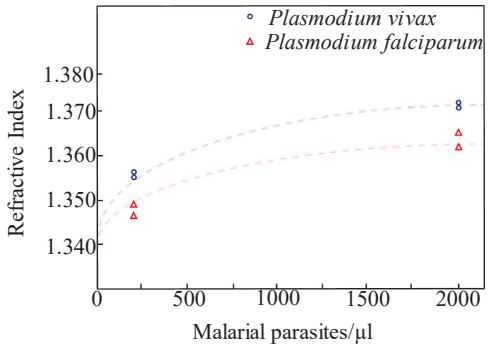

Fig. 8. Comparison of refractive index of whole blood samples (F01–3, F01–4, F06–3, F06–4, V01–3, V01–4, V06–3 and V06–4) with various concentrations of malarial parasites *Plasmodium vivax* and *Plasmodium falciparum* shown in blue (circles) and red (triangles) respectively. Backdrop shows the calibration curves in red and blue for *Plasmodium falciparum* and *Plasmodium vivax* respectively as obtained from Fig. 5 (Section 2.4).

infection as part of this study.

3. Conclusion

We developed a refractive index-based surface plasmon microscope to study malarial species in whole blood. We successfully demonstrated that the microscope can be used for the detection, quantification and distinction of two malarial species *Plasmodium falciparum* and *Plasmodium vivax* which are rampant in Asia and Africa. Further, we also showcased the effectiveness of the developed microscope for analyzing low parasitemia (~60 parasites/μl) with reliable reproducibility of results. It should be noted that varying results may be obtained in the case of co-infections (for instance fevers induced by Plasmodium *falciparum* might activate dormant Plasmodium *vivax* parasites). We believe performing pilot study with a large cohort will be required to satisfy such a quest in the future. We are currently in the process of collecting whole blood samples from Nigeria with mixed infections occurring from both *Plasmodium falciparum* and *Plasmodium vivax* for the cohort study which is currently out of scope for this work and will be reported elsewhere.

Funding

A part of this work was supported by funds provided by Humboldt Foundation, Germany. Open Access funding enabled and organized by Project DEAL.

CRediT authorship contribution statement

Andreas Offenhäusser: Writing – review & editing, Conceptualization. **Ipsita Chakraborty:** Writing – original draft, Project administration, Methodology, Investigation, Formal analysis, Data curation, Conceptualization. **Justus Bednar:** Software.

Declaration of Competing Interest

The authors declare that they have no known competing financial interests or personal relationships that could have appeared to influence the work reported in this paper.

Acknowledgements

I.C. is supported by a fellowship from the Alexander von Humboldt Foundation, Germany. We thank Dr. Gabriela Figueroa-Miranda, IBI-3, Forschungszentrum Jülich GmbH, Germany, and Dr. Katherine Torres, Lab. Malaria, Universidad Peruana Cayetano Heredia, Peru for kindly providing human whole blood samples with various plasmodium species. We thank Michael Prömpers, IBI-3, Forschungszentrum Jülich GmbH, Germany, for the fabrication of the metallic substrates. We also thank Yifan Xu, JNCS-2, Forschungszentrum Jülich GmbH, Germany, for performing the XRR of the metallic substrate.

Data availability

Data will be made available on request.

References

[1] World Health Organization. World malaria report 2023. WHO Geneva. Technical report at https://www.who.int/publications/i/item/9789240086173, 2023.
[2] Gunjan Arora, Yu-Min Chuang, Photini Sinnis, George Dimopoulos, Erol Fikrig, Malaria: influence of anopheles mosquito saliva on plasmodium infection, ISSN 1471-4906, Trends Immunol. 44 (4) (2023) 256–265, https://doi.org/10.1016/j.it.2023.02.005.
[3] Mattea Scheiner, Paul-christian burda and alyssa ingmundson "moving on: how malaria parasites exit the liver, Mol. Microbiol. 121 (2024) 328–340.
[4] H. Patel, N.K. Minkah, S. Kumar, et al., Malaria blood stage infection suppresses liver stage infection via host-induced interferons but not hepcidin, Nat. Commun. 15 (2024) 2104, https://doi.org/10.1038/s41467-024-46270-3.
[5] Spinello Antinori, Andrea Giacomelli, Giacomo Casalini, Anna Lisa Ridolfo, How to manage adult patients with malaria in the non-endemic setting, ISSN 1198-743X, Clin. Microbiol. Infect. (2024), https://doi.org/10.1016/j.cmi.2024.06.021.
[6] O.C. Villena, A. Arab, C.A. Lippi, et al., Influence of environmental, geographic, socio-demographic, and epidemiological factors on presence of malaria at the community level in two continents, Sci. Rep. 14 (2024) 16734, https://doi.org/10.1038/s41598-024-67452-5.
[7] G. Madhu, A.W. Mohamed, S. Kautish, et al., Intelligent diagnostic model for malaria parasite detection and classification using imperative inception-based capsule neural networks, Sci. Rep. 13 (2023) 13377, https://doi.org/10.1038/s41598-023-40317-z.
[8] Ben-Zion Katz, Shahar Karny, Pursuing the elusive footsteps of malaria in peripheral blood smears utilizing artificial intelligence, 00:1–2, Br. J. Haematol. (2024), 00:1–2.
[9] A. Acherar, X. Tannier, I. Tantaoui, J.-Y. Brossas, M. Thellier, R. Piarroux, Evaluating Plasmodium falciparum automatic detection and parasitemia estimation: A comparative study on thin blood smear images, pone.0304789, PLoS ONE 19 (6) (2024) e0304789, https://doi.org/10.1371/journal. pone.0304789.
[10] E. Aninagyei, J.G. Deku, K.T. Yemofio, E. Quainoo, K.A. Ntiri, E. Yaro, et al., Comparative evaluation of the diagnostic accuracies of four different malaria rapid diagnostic test kits available in Ghana, PLoS ONE 19 (5) (2024) e0302840.
[11] Jiran Li, Alexuse M. Saidi, Karl Seydel, Peter B. Lillehoj, Rapid diagnosis and prognosis of malaria infection using a microfluidic point-of-care immunoassay, Biosens. Bioelectron. 250 (2024) 116091, https://doi.org/10.1016/j.bios.2024.116091.
[12] Meng Yee Lai, Sasheela Sri La. Sri Ponnampalavanar, Sharifah Faridah Syed Omar, Yee Ling Lau, A visualized hybrid PCR-LAMP assay for the detection of human Plasmodium species, ISSN 0001-706X, Acta Trop. 251 (2024) 107120. ISSN 0001-706X.
[13] T.K. Nguyen, H. Jun, J.M. Louis, E. Mazigo, W.-J. Lee, H.C. Youm, et al., Enhancing malaria detection in resource-limited areas: a high-performance colorimetric LAMP assay for Plasmodium falciparum screening, e0298087, PLoS ONE 19 (2) (2024), https://doi.org/10.1371/journal.
[14] H. Gupta, S. Sharma, I. Gilyazova, et al., Molecular tools are crucial for malaria elimination, Mol. Biol. Rep. 51 (2024) 555, https://doi.org/10.1007/s11033-024-09496-4.
[15] Van Schuijlenburg, et al., Ageing of Plasmodium falciparum malaria sporozoites alters their motility, infectivity and reduces immune activation in vitro, Malar. J. 23 (2024) 111, https://doi.org/10.1186/s12936-024-04946-7.
[16] V. Chaumeau, M. Piarroux, T. Kulabkeeree, S. Sawasdichai, A. Inta, W. Watthanaworawit, et al., Identification of Southeast Asian Anopheles mosquito species using MALDI-TOF mass spectrometry, PLoS ONE 19 (7) (2024) e0305167, https://doi.org/10.1371/journal.pone.0305167.
[17] Gabriela Figueroa-Miranda, Lingyan Feng, Simon Chi-Chin Shiu, Roderick Marshall Dirkzwager, Yee-Wai Cheung, Julian Alexander Tanner, Michael Josef Schöning, Andreas Offenhäusser, Dirk Mayer, Aptamer-based electrochemical biosensor for highly sensitive and selective malaria detection with adjustable dynamic response range and reusability, Sens. Actuators B Chem. 255 (Part 1) (2018) 235–243, https://doi.org/10.1016/j.snb.2017.07.117.
[18] V.S. Chaudhary, D. Kumar, S. Kumar, Gold-immobilized photonic crystal fiber-based SPR biosensor for detection of malaria disease in human body, IEEE Sens J. 21 (16) (2020) 17800–17807, https://doi.org/10.1109/JSEN.2021.
[19] W. Zhang, R. Singh, F.-Z. Liu, C. Marques, B. Zhang, S. Kumar, WaveFlex biosensor: a flexible-shaped plasmonic optical fiber sensor for histamine detection, 1 Oct.1, IEEE Sens. J. 23 (19) (2023) 22533–22542, https://doi.org/10.1109/JSEN.2023.3305464, 1 Oct.1.
[20] Qi Zhang, Chaofan Gu, Ragini Singh, Sourabh Jain, Ray T. Chen, Bingyuan Zhang, Santosh Kumar, Hump-shaped seven-core fiber-based WaveFlex biosensor for rapid detection of glyphosate pesticides in real food samples, Opt. Express 32 (2024) 25789–25804.
[21] Rajan Jha, Pratik Mishra, Santosh Kumar, Advancements in optical fiber-based wearable sensors for smart health monitoring, ISSN 0956-5663, Biosens. Bioelectron. 254 (2024) 116232, https://doi.org/10.1016/j.bios.2024.116232.
[22] X. Liu, R. Singh, G. Li, C. Marques, B. Zhang, S. Kumar, WaveFlex biosensor-using novel tri-tapered-in-tapered four-core fiber with multimode fiber coupling for detection of aflatoxin B1, 15 Dec.15, J. Light. Technol. 41 (24) (2023) 7432–7442, https://doi.org/10.1109/JLT.2023.3301069.
[23] H. Raether, Surface Plasmons on Smooth and Rough Surfaces and on Gratings, Springer, Berlin, 1988.
[24] H. Kano, S. Mizuguchi, S. Kawata, Excitation of surface-plasmon polaritons by a focused laser beam, J. Opt. Soc. Am. B 15 (1998) 1381.
[25] I. Chakraborty, D. Matsubayashi, T. Omachi, Y. Hasegawa, H. Kano, Optimization of substrate to culture and image live cells for surface plasmon microscopy, 122020E, Proc. Spie. 12202 (2022), 122020E.
[26] Akinari Abe, Ipsita Chakraborty, Daiki Matsubayashi, Tsuyoshi Noguchi, Akitoshi Okino, Hiroshi Kano, Deposition of a polymer thin film on a silver surface for surface plasmon sensing, Jpn. J. Appl. Phys. 63 (2024) 062004.
[27] Ipsita Chakraborty, Akinari Abe, et al., Refractive index measurement of myelinated co-cultured DRG neurons with surface plasmon microscopy. 13th International Proceedings of Optics and Photonics International Congress (OPIC, OPIE, Yokohama, Japan, 2024, p. 37, https://doi.org/10.1117/12.3058965.
[28] Ipsita Chakraborty, Hiroshi Kano, Microscopic-characterization of photoinduced birefringence of azo-polymer thin film by focused surface plasmon, Opt. Laser Technol. 147 (2022) 107673, https://doi.org/10.1016/j.optlastec.2021.107673.
[29] Ipsita Chakraborty, Hiroshi Kano, Characterization of cellophane birefringence due to uniaxial strain by focused surface plasmon microscopy, OSA Contin. 4 (2021) 409–415, https://doi.org/10.1364/OSAC.417743.
[30] Ipsita Chakraborty and Hiroshi Kano Low birefringence measurement with focused surface plasmon towards label free detection of dermatoheliosis, Proc. SPIE 11661, Plasmonics in Biology and Medicine XVIII, 116610D (2021); https://doi.org/10.1117/12.2582876.
[31] Ipsita Chakraborty and Hiroshi Kano "Near-field chicken skin analysis with focused surface plasmon", Proc. SPIE 11921, Emerging Technologies for Cell and Tissue Characterization, 119210H (2021); https://doi.org/10.1117/12.2615635.
[32] Ipsita Chakraborty and Hiroshi Kano Salivary refractive index dependence on circadian rhythm with focused surface plasmon, Proc. SPIE 12854, Label-free Biomedical Imaging and Sensing (LBIS) 2024, 128540E; https://doi.org/10.1117/12.3002528 (2024).
[33] Ipsita Chakraborty, Justus Bednar, Andreas Offenhäusser, Detecting malaria with surface plasmon microscope, Proc. SPIE 13008 Biophotonics PointCare III (2024) 1300806, https://doi.org/10.1117/12.3017053.
[34] J. Ning, K. Nagata, A. Ainai, H. Hasegawa, H. Kano, Detection of influenza virus with specific subtype by using localized surface plasmons excited on a flat metal surface (Article), Jpn. J. Appl. Phys. 52 (2013) 082402.
[35] I. Chakraborty, A. Abe, D. Matsubayashi, H. Kano, Dynamic refractive index analysis by focused surface plasmon for continuous evaluation of evaporation of saliva. 2022 Conference on Lasers and Electro-Optics Pacific Rim (CLEO-PR), Sapporo, Japan, 2022, pp. 1–2, https://doi.org/10.1109/CLEO-PR62338.2022.10432131.
[36] A. Glavic, M. Bjorck, GenX 3: the latest generation of an established tool, J. Appl. Cryst. 55 (2022) 1063–1071.
[37] M. Born, E. Wolf. Principles of Optics: Electromagnetic Theory of Propagation, Interference and Diffraction of Light, 7th edn., Cambridge University Press, Cambridge, 1999, p. 55. Chapter 1.6.
[38] Bednár, J. (2025). SPRManalysis-2 (2.3.8). Zenodo. https://doi.org/10.5281/zenodo.13140709.

Ipsita Chakraborty studied optics and completed her dissertation in 2021 at Muroran Institute of Technology Japan with JSPS-MEXT. Then she moved to the National Institute

of Natural Sciences (NINS), Japan for a brief period. After which she received the Alexander von Humboldt fellowship in 2023 and joined Forschungszentrum Jülich, Germany for her research work. Her research interests include the development of label-free optical probes for preclinical disease detection with inherent physical properties like refractive index and linear/circular birefringence.

Justus Bednar is a doctoral researcher in the Institute of Biological Information Processing (IBI-3) at Forschungszentrum Jülich and Rheinisch-Westfälische Technische Hochschule (RWTH) Aachen. He completed his bachelors and masters in physics from RWTH Aachen in 2018 and 2020 respectively.

Andreas Offenhäusser studied physics and completed his dissertation in 1989 at the University of Ulm. For 2 years he worked in the field of power transistors at Robert Bosch GmbH in Reutlingen, Germany. From 1992 until 1994 he performed a post doctoral study at the Frontier Research Program at RIKEN, Japan. Afterwards, he worked as a group leader at the Max-Planck-Institute for Polymer Research in Mainz, Germany. Since 2001, Offenhäusser is director at the Institute of Biological Information Processing (IBI-3) at Forschungszentrum Jülich and Professor of Experimental Physics at the Rheinisch-Westfälische Technische Hochschule (RWTH) Aachen. His research interest includes micro/nano-electronics for Life-Sciences, i.e. how micro/nano electronic systems can help to solve important problems in life sciences. Examples include integrated devices for detection of cell response, DNA, proteins, and small molecules and life-Sciences for micro/nano electronic systems, i.e. how we can learn from nature to build micro and nano electronic devices. Examples include protein mediated electronic devices and neuro-electronic circuitries.